Advances in Medical Physics and Applied Sciences

Original Article
DOI: https://doi.org/10.63187/ampas.31
Adv Med Phy App Sci, 2025; 1(2):45-52

Investigating the Temporal Stability of 3D-Printed PLA Samples under Ambient Storage Conditions

ÖZSOYKAL, İsmail [1], YURT, Ayşegül [1,2,3], SELVER, Mustafa Alper [1,3]

[1] *Bioizmir, Dokuz Eylul University, Balcova, Izmir, Türkiye.*
[2] *Department of Medical Physics, Health Sciences Institution, Dokuz Eylul University, Izmir, Türkiye.*
[3] *Electrical and Electronics Engineering Deparment, Dokuz Eylul University, Izmir, Türkiye.*

Correspondence:
İsmail ÖZSOYKAL Bioizmir, Dokuz Eylul University, Izmir, Türkiye.
ozsoykal@gmail.com

Received: *3 February 2025*
Revised: *15 April 2025*
Accepted: *10 May 2025*

ABSTRACT

Purpose: This study aims to evaluate the longitudinal radiological stability of 3D-printed PLA-based materials under ambient storage conditions, with varying infill densities and flow rates, in order to understand the impact of these factors on their use in medical imaging and radiation therapy. Methodology: Twenty-five cylindrical samples were 3D printed using three PLA-based filaments (Lightweight PLA, Premium PLA, and StoneFil), with varying infill densities and flow rates. The samples were stored in ambient room conditions, and their radiological properties were measured over a 6-month period using CT scans. Hounsfield Unit (HU) values were analyzed using a leave-one-out approach and linear regression analysis to assess temporal stability and the relationship between printing parameters and HU values. Findings: The results demonstrated minimal variations in HU values, with most measurements falling within the limits of agreement, indicating stable radiological properties across all filament types. A strong linear correlation was observed between printing parameters and HU values ($R^2 > 0.99$). Conclusion: The study confirms the stability of 3D-printed PLA-based materials in typical environmental conditions over a 6-month period. These findings support the use of 3D-printed phantoms in medical applications, although further research is needed to explore the effects of UV exposure, higher levels of humidity, and other environmental factors on long-term material stability.

Keywords: *3D Printing, Phantom, Stability, computed tomography.*

INTRODUCTION

Three-dimensional (3D) printing is an advanced manufacturing technology that enables the creation of customizable solutions across various disciplines. In the field of medical physics, its adoption has grown significantly, with a growing body of research highlighting the development of 3D-printed test tools—commonly referred to as phantoms—for use in diagnostic imaging and radiation therapy. These phantoms play a vital role in improving the accuracy, efficiency, and quality assurance of procedures within radiology and radiation oncology departments [1,2].

Fused Deposition Modeling (FDM) is among the most widely used 3D printing technologies. It functions by extruding melted thermoplastic filament layer by layer to construct a three-dimensional object. A wide range of materials can be used in FDM printing, including polylactic acid (PLA), acrylonitrile butadiene styrene (ABS), and polyethylene terephthalate glycol (PETG), with PLA being among the most commonly used due to its ease of use and biocompatibility. FDM has proven particularly valuable in radiation-related applications for fabricating customized phantoms and anatomical models used in dosimetry, radiation shielding, and treatment planning [1,3–6].

The impact of environmental factors such as temperature and humidity on the dimensional stability and mechanical performance of 3D-printed components has become a significant area of research. While temperature is widely recognized as a major contributor to deformation, humidity—through moisture absorption—also plays a critical role in altering the structural integrity of 3D-printed materials.

Moisture uptake can lead to dimensional changes and deterioration of mechanical properties. For example, Onyx parts exposed to humidity substantially decreased Young's modulus, with reductions up to 65% after prolonged exposure [7]. Similarly, in nylon-

based materials, moisture absorption has been shown to cause dimensional changes of approximately 0.5–1.5%, with height being the most affected dimension [8].

PLA-based composite filaments have demonstrated superior resistance to moisture-induced degradation compared to ABS and nylon [9]. However, similar to other materials, PLA's mechanical properties also degrade with increasing relative humidity. In addition, Demirtaş et al. reported that the dimensional accuracy of 3D-printed specimens is more adversely affected by humidity when printed with lower infill percentages [10].

Despite the growing understanding of mechanical and geometrical degradation under environmental stressors, few studies have investigated the radiological implications of these changes over time. In a study by Brunner et al., PLA samples printed with 100% infill maintained radiological stability over a 12-month period [11]. However, to the best of our knowledge, no studies have assessed the radiological stability of FDM-printed parts with lower infill percentages.

This study aims to investigate the potential impact of ambient storage conditions on the longitudinal stability of PLA-based 3D-printed materials fabricated with varying infill densities and flow rate settings—two parameters that influence the internal air content and, consequently, the material's susceptibility to moisture absorption.

MATERIAL AND METHODS

3D Printing of Samples

Twenty-five cylindrical samples were 3D printed using three distinct polylactic acid (PLA)-based filaments: Lightweight PLA (LW-PLA) by ColorFabb, Premium PLA by Raise3D, and StoneFil by FormFutura. According to the manufacturers, the physical densities of PLA and LW-PLA are both 1.2 g/cm³, while StoneFil has a higher density of 1.4 g/cm³.

Samples were printed using a Raise3D Pro3 Plus 3D printer. Each sample was fabricated with identical dimensions of 15 mm in diameter and 10 mm in height. Printing parameters—including temperature, flow rate, and infill percentage—were individually optimized for each filament type to achieve a broad range of material densities corresponding to a wide spectrum of Hounsfield Unit (HU) values.

For PLA and StoneFil samples, physical density was controlled by progressively reducing the infill percentage. In contrast, the density of LW-PLA samples was modulated by lowering the flow rate while printing at an elevated temperature of 250 °C. This approach leverages the material's unique foaming behavior under heat, enabling low-density fabrication without relying on low infill rates [12]. However, this method also introduces microscopic air bubbles within the printed structure, which may increase the material's susceptibility to moisture absorption over time.

The detailed parameters used in the printing process are summarized in Table 1.

Table 1. Printing parameters for the filaments used to print cylindrical samples.

(*: increased in increments of 5%, **: increased in increments of 10%)

	LW-PLA	PLA	Stonefil
Temperature (°C)	250	205	220
Infill Rate (%)	100	55-100*	75-100*
Flow Rate (%)	20-60**	100	100
Speed (mm/s)	40	40	40

As shown in Table 1, nine LW-PLA samples were printed with flow rates ranging from 20% to 60%, in 5% increments. For all LW-PLA samples, the printing temperature, infill rate, and printing speed were fixed at 250 °C, 100%, and 40 mm/s, respectively. In contrast, PLA samples were printed at a temperature of 205 °C, with a constant flow rate of 100% and a printing speed of 40 mm/s. Ten different infill rates—ranging from 55% to 100% in 5% increments—were used to produce ten distinct PLA samples. StoneFil samples were printed at 220 °C, 100% flow rate, and 40 mm/s. Their densities were adjusted by varying the infill rate between 75% and 100%, also in 5% increments.

After printing, all sample groups for the three filaments were mounted in cylindrical hollows within three blocks. As shown in Figure 1, the blocks were arranged consecutively along the longitudinal axis of the CT scanner for imaging.

After printing, all sample groups for the three filaments were mounted in cylindrical hollows within three blocks. As shown in Figure 1, the blocks were then positioned consecutively and parallel to each other, with the intention of aligning them along the longitudinal axis of the CT scanner during imaging.

Storage Conditions and Measurements

The samples were printed on September 20, 2024, and stored under ambient room conditions without any protective measures throughout the study. The Lufft Opus 20 climate and environmental monitoring system monitored temperature, humidity, and air pressure every ten minutes.

CT Scanning of the Samples

Samples underwent a total of 9 CT scans conducted on various dates between 27.09.2024 and 26.03.2025, making up a 6-month period. All scans were performed using a single 64-slice CT scanner, Philips 5000 Ingenuity. Scan parameters are 120 kVp, 360 mAs, 1 mm, and 300 mm for tube voltage, effective tube current, slice thickness, and field of view (FOV), respectively.

Data Collection and Statistical Analysis

The mean Hounsfield Unit (HU) values for each sample were determined by placing a 10 mm diameter circular region of interest (ROI) at the center of the sample, as illustrated in Figure 2, and calculating the average HU across five consecutive CT slices.

The temporal stability of CT attenuation for each sample was analyzed using a leave-one-out (LOO) approach. For each measurement, the difference from the mean of the remaining eight measurements was calculated and plotted against their average. This method enables the assessment of within-sample agreement while minimizing the impact of individual outliers. The analysis was performed separately for each sample, and the results were presented in combined Bland-Altman plots, with color-coded points and sample-specific limits of agreement (LoA) defined as 1.96 times the standard deviation (SD) of the mean measurements.

Additionally, linear regression analysis was performed to explore the relationship between printing parameters — infill rate for Stonefil and PLA, and flow rate for LW-PLA — and the mean HU values of the samples.

Figure 1: Characteristics of the detectors used for measurements.

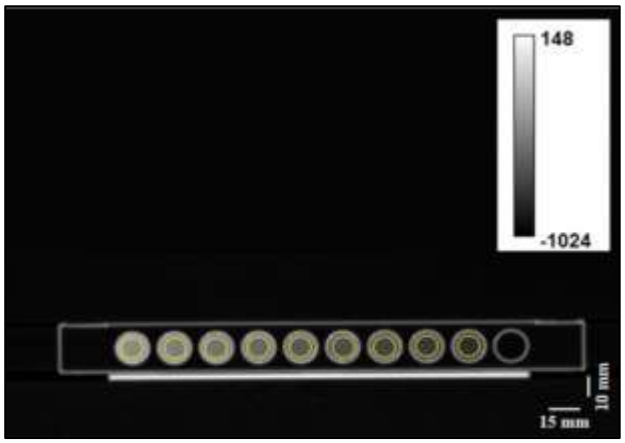

Figure 2a: Characteristics of the detectors used for measurements.

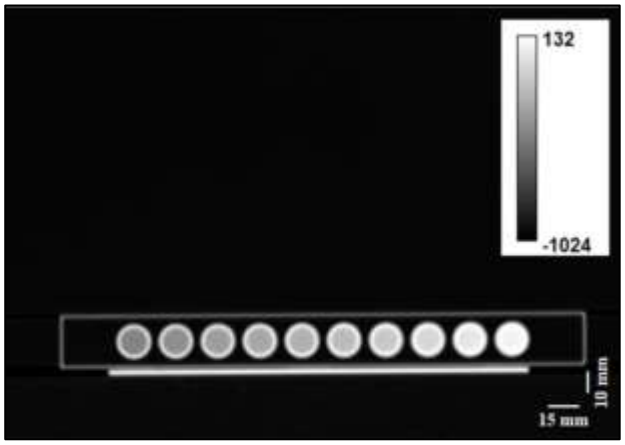

Figure 2b: Characteristics of the detectors used for measurements.

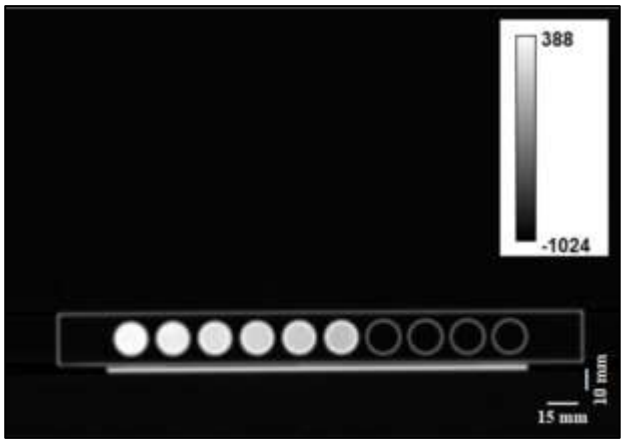

Figure 2c: Characteristics of the detectors used for measurements.

RESULTS

Storage conditions recorded for the study period is given in figure 3 and the descriptive statistics of the measured data is given in table 2.

Table 2. Descriptive statistics of the measured storage conditions.

	Temperature (°C)	Relative Humidity (%)	Relative Air Pressure (hPa)
Average	21.2	44.8	1015.3
Minimum	16.8	20.8	996.8
Maximum	30.6	60.4	1029.9
Standard Deviation	2.5	8.8	5.8

Tables 3, 4, and 5 present the measured mean HU values and SD for Stonefil, PLA, and LW-PLA samples, respectively, arranged in descending order of mean HU. The highest recorded HU value, approximately 400 HU, was observed in the Stonefil sample printed with 100% infill, while the lowest, around -820 HU, corresponded to the LW-PLA sample printed with a 20% flow rate.

The results of the LOO analysis for each group of filament samples are presented in Figures 4, 5, and 6. For the Stonefil samples, measurement #9 of the 100% infill sample showed a deviation of -0.50 HU, slightly below the lower limit of agreement (LoA). Similarly, measurement #9 of the 80% infill sample exhibited a smaller negative deviation of -0.23 HU, also below the lower LoA but to a lesser extent. In contrast, measurement #9 of the 75% infill sample demonstrated a positive deviation of +0.15 HU, lying just above the upper LoA—still within a narrow range that may be considered a mild outlier.

Table 3. Mean HU±SD of Stonefil samples printed with different infill rates (%) and measured at different dates.

Sample #	Infill Rate (%)	Measurement #								
		1	2	3	4	5	6	7	8	9
1	100	402±4	400±4	401±4	401±4	403±4	398±5	400±5	402±5	395±5
2	95	328±5	330±4	334±6	331±4	334±4	330±5	328±6	331±4	325±7
3	90	246±6	250±5	249±4	252±6	247±5	246±4	248±7	249±5	243±8
4	85	154±3	154±4	154±4	156±3	153±5	150±5	152±5	154±4	148±7
5	80	93±4	92±6	93±6	95±5	96±7	91±4	93±5	94±4	88±7
6	75	27±3	27±5	28±5	28±4	26±4	27±6	26±5	28±5	30±7

Table 4. Mean HU±SD of PLA samples printed with different infill rates (%) and measured at different dates.

Sample #	Infill Rate (%)	Measurement #								
		1	2	3	4	5	6	7	8	9
1	100	60±5	63±4	59±6	58±7	59±5	65±7	64±4	60±6	66±5
2	95	-4±5	-2±5	-6±6	-4±4	-3±4	-6±5	0±6	3±5	5±7
3	90	-73±3	-65±2	-71±4	-71±5	-73±4	-67±7	-72±4	-70±6	-63±5
4	85	-135±4	-130±1	-135±2	-131±4	-134±3	-130±6	-135±4	-132±5	-128±3
5	80	-200±6	-196±4	-201±3	-200±5	-199±4	-195±7	-200±5	-193±7	-194±5
6	75	-237±8	-237±4	-237±8	-235±8	-239±3	-235±9	-239±6	-230±7	-234±7
7	70	-282±5	-281±2	-283±2	-283±2	-281±2	-280±5	-279±5	-281±5	-278±4
8	65	-323±3	-321±1	-323±1	-324±2	-322±1	-320±5	-322±4	-322±3	-317±3
9	60	-383±4	-387±3	-387±4	-388±5	-388±3	-385±4	-386±4	-387±4	-380±4
10	55	-429±8	-432±4	-435±5	-430±5	-434±5	-430±5	-425±4	-434±4	-429±3

Table 5. Mean HU±SD of LW-PLA samples printed with different flow rates (%) and measured at different dates.

Sample #	Flow Rate (%)	Measurement #								
		1	2	3	4	5	6	7	8	9
1	60	-385±3	-387±3	-384±3	-385±5	-384±4	-384±4	-388±5	-385±4	-385±6
2	55	-439±1	-437±2	-437±5	-437±2	-435±3	-435±4	-437±7	-436±5	-439±6
3	50	-499±3	-497±5	-498±3	-496±4	-495±5	-497±5	-495±4	-498±6	-498±5
4	45	-559±5	-553±5	-557±2	-559±5	-554±4	-550±7	-550±6	-555±7	-554±7
5	40	-623±2	-612±1	-622±2	-621±2	-618±3	-617±6	-614±6	-614±6	-622±5
6	35	-674±2	-672±2	-675±4	-674±3	-676±3	-668±5	-669±7	-673±7	-675±6
7	30	-721±2	-724±3	-721±3	-723±4	-720±4	-716±5	-719±5	-722±4	-724±5
8	25	-770±4	-771±3	-771±5	-766±4	-768±3	-769±5	-766±6	-768±6	-772±5
9	20	-819±3	-819±3	-816±4	-816±3	-819±4	-818±5	-817±6	-815±5	-820±4

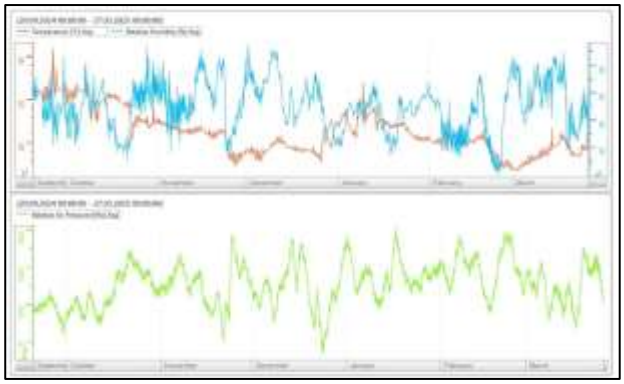

Figure 3: Characteristics of the detectors used for measurements.

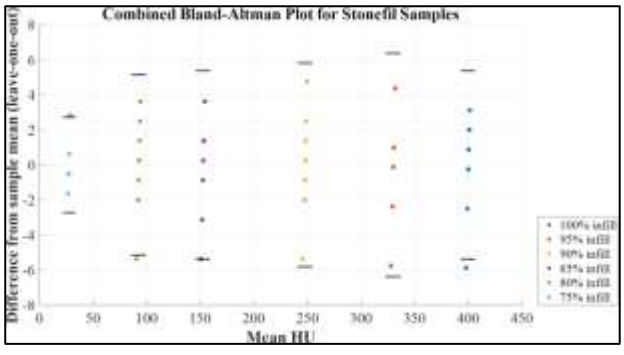

Figure 4: Characteristics of the detectors used for measurements.

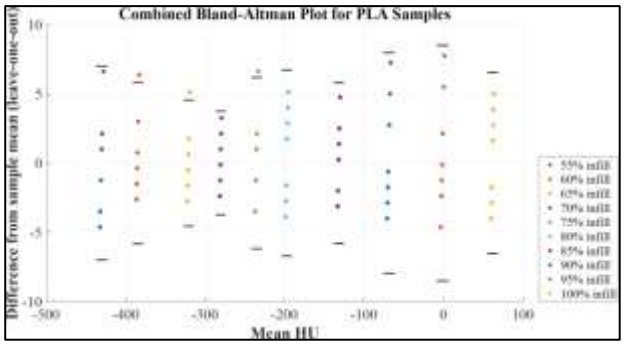

Figure 5: Characteristics of the detectors used for measurements.

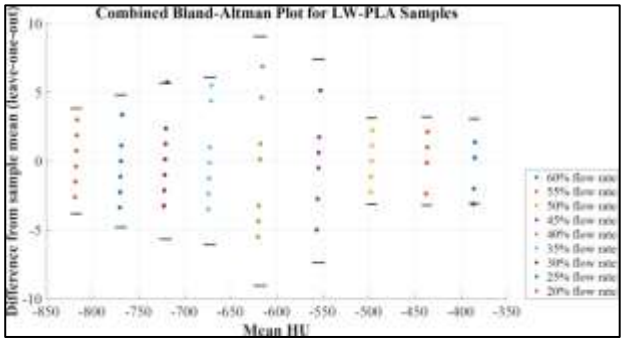

Figure 6: Characteristics of the detectors used for measurements.

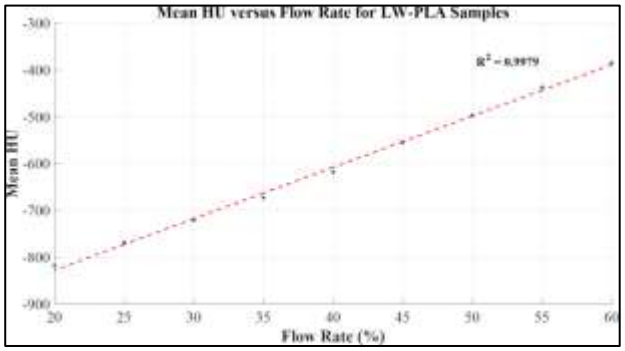

Figure 7: Characteristics of the detectors used for measurements.

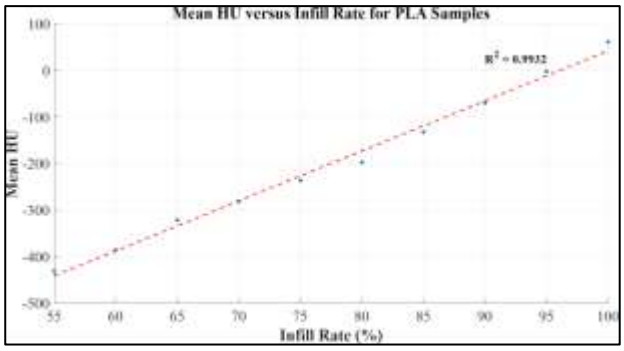

Figure 8: Characteristics of the detectors used for measurements.

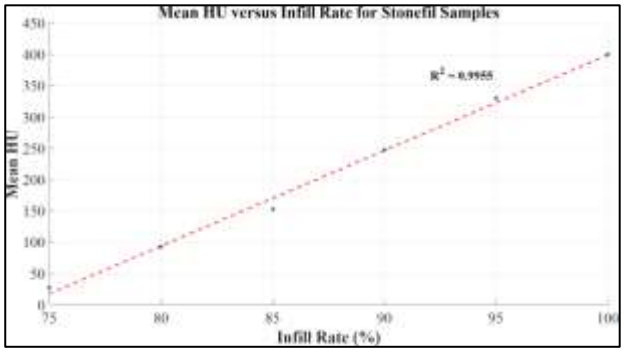

Figure 9: Characteristics of the detectors used for measurements.

For the PLA samples, measurement #9 of the 60% infill sample showed a deviation of +0.54 HU, placing it slightly above the upper limit of agreement (LoA) and identifying it as an outlier with a moderate deviation from expected values. Similarly, measurement #9 of the 65% infill sample had a deviation of +0.56 HU, also exceeding the upper LoA by a comparable margin, indicating another mild outlier. Finally, measurement #8 of the 75% infill sample displayed a smaller deviation of +0.44 HU, slightly above the upper LoA, and can also be considered a mild outlier.

For the LW-PLA samples, measurement #7 of the 60% flow rate sample showed a deviation of -0.05 HU, slightly below the lower limit of agreement (LoA), indicating a very minor deviation and classifying it as a mild outlier. Similarly, measurement #6 of the 30% flow rate sample exhibited a deviation of +0.08 HU, just above the upper LoA, also representing a small deviation and suggesting a minor outlier for this sample.

Figure 7, figure 8 and figure 9 shows the findings of linear regression analysis, where strong linear correlation is observed between printing parameters and mean HU of samples printed by all three filaments (R^2>0.99).

DISCUSSION

In recent years, the use of 3D-printed materials in radiological applications—particularly for phantom production—has gained considerable attention due to the flexibility, affordability, and customization offered by additive manufacturing. However, despite growing interest, relatively few studies have investigated the time-dependent radiological stability of these materials under varying print and storage conditions. In one such study, prints with an infill rate of 100%—corresponding to a limited HU range—were analyzed and the results demonstrated that FDM printed parts maintained stability at the end of a 12 month period [11].

In this study, we assessed the time stability of 3D prints produced at varying infill and flow rates using three PLA-based filaments from different vendors. The prints were stored under ambient room conditions without specific control measures. The environmental conditions during the CT measurement period are summarized in Figure 3, with descriptive statistics provided in Table 2. The average temperature was 21.2°C, with a minimum of 16.8°C and a maximum of 30.6°C. Relative humidity averaged 44.8%, ranging from 20.8% to 60.4%. The average relative air pressure was 1015.3 hPa, with a minimum of 996.8 hPa and a maximum of 1029.9 hPa. Standard deviations for temperature, relative humidity, and air pressure were 2.5°C, 8.8%, and 5.8 hPa, respectively, reflecting moderate variability in environmental conditions.

Figures 7, 8, and 9, shows the resulting HU values that cover a wide range—from approximately +400 HU to -820 HU—encompassing the radiological properties of various soft tissues, including the lungs, as well as spongy bone. In addition, the linear regression analysis indicated strong linear relationships for all three sample groups (R2>0.99).

A leave-one-out analysis was conducted to evaluate the impact of individual data points on the overall trend. This method quantifies how each measurement deviates from the mean of the remaining data, helping to identify potential outliers or inconsistencies. The results are displayed in a Bland–Altman plot, illustrating the agreement between each data point and the mean of the others, and highlighting any deviations or systematic discrepancies. These deviations are expressed in

Hounsfield Units (HU), representing the difference between each sample's measured HU and the mean of the remaining measurements in terms of the limits of agreement (LoA).

Figures 4, 5, and 6 reveal that, out of a total of 225 measurements (25 samples × 9 measurements per sample), 8 measurements fall outside the LoA, either above or below. These deviations range from 0.05 HU to 0.56 HU, considered minimal. These results suggest that measurements taken over the 6-month period remained stable across different sample densities, with variations attributable to differences in filament types and printing parameters.

There are several limitations to this study. First, no control group was established to evaluate the impact of factors such as increased humidity, which could have led to different findings. Second, pre- and post-measurements of the dimensions and weight of the samples were not included, which would have provided a more comprehensive analysis of physical changes over time. However, it is important to note that variations in these parameters would also affect the final HU measurements. Lastly, the study did not test the effects of UV light exposure on the materials, which could potentially influence the long-term stability of the printed samples. Despite these limitations, this study contributes to the growing body of knowledge on using 3D-printed materials in medical applications, particularly in producing customizable phantoms for radiation therapy and diagnostic imaging.

CONCLUSION

This study provides valuable insights into the impact of ambient storage conditions on the radiological stability of 3D-printed PLA-based materials with varying infill densities and flow rates. The findings suggest that, under typical environmental conditions, the radiological properties of FDM-printed materials remain relatively stable over a six-month period. While the study demonstrates the robustness of PLA-based materials, further research is needed to assess the effects of additional environmental factors, such as UV exposure and higher humidity levels, on long-term stability. Additionally, incorporating pre- and post-measurements of sample dimensions and weight and introducing control groups would provide a more comprehensive understanding of the material's behavior under different conditions.

Conflict of Interest

There are no conflicts of interest and no acknowledgements.

ACKNOWLEDGEMENT

This study was funded by the TÜBİTAK 1005 project no: 123R064, and TÜBİTAK 1001 project no:123R036.

References

1. Tino R, Yeo A, Leary M, Brandt M, Kron T. A systematic review on 3D-Printed imaging and dosimetry phantoms in radiation therapy. Technol Cancer Res Treat 2019;18:1–14. https://doi.org/10.1177/1533033819870208 .

2. Filippou V, Tsoumpas C. Recent advances on the development of phantoms using 3D printing for imaging with CT, MRI, PET, SPECT, and ultrasound. Med Phys 2018;45:e740–60. https://doi.org/10.1002/mp.13058.

3. Jreije A, Mutyala SK, Urbonavičius BG, Šablinskaitė A, Keršienė N, Puišo J, et al. Modification of 3D Printable Polymer Filaments for Radiation Shielding Applications. Polymers (Basel) 2023;15. https://doi.org/10.3390/polym15071700.

4. Ceh J, Youd T, Mastrovich Z, Peterson C, Khan S, Sasser TA, et al. Bismuth infusion of ABS enables additive manufacturing of complex radiological phantoms and shielding equipment. Sensors (Switzerland) 2017;17:1–11. https://doi.org/10.3390/s17030459.

5. Lee MY, Han B, Jenkins C, Xing L, Suh TS. A depth-sensing technique on 3D-printed compensator for total body irradiation patient measurement and treatment planning. Med Phys 2016;43:6137–44. https://doi.org/10.1118/1.4964452.

6. Zhao Y, Moran K, Yewondwossen M, Allan J, Clarke S, Rajaraman M, et al. Clinical applications of 3-dimensional printing in radiation therapy. Medical Dosimetry 2017;42:150–5. https://doi.org/10.1016/j.meddos.2017.03.001.

7. Nikiema D, Balland P, Sergent A. Study of the Mechanical Properties of 3D-printed Onyx Parts: Investigation on Printing

Parameters and Effect of Humidity. Chinese Journal of Mechanical Engineering: Additive Manufacturing Frontiers 2023;2:100075. https://doi.org/10.1016/j.cjmeam.2023.100075.

8. Faust JL, Kelly PG, Jones BD, Roy-Mayhew JD. Effects of coefficient of thermal expansion and moisture absorption on the dimensional accuracy of carbon-reinforced 3D printed parts. Polymers (Basel) 2021;13. https://doi.org/10.3390/polym13213637.

9. Banjo AD, Agrawal V, Auad ML, Celestine ADN. Moisture-induced changes in the mechanical behavior of 3D printed polymers. Composites Part C: Open Access 2022;7. https://doi.org/10.1016/j.jcomc.2022.100243.

10. Demirtaş MS, Avcıoğlu E. Ambient relative humidity effects on mechanical properties of FDM 3D printed PLA components. Phys Scr 2023;98. https://doi.org/10.1088/1402-4896/accfcf.

11. Brunner J, Langgartner L, Danhel H, Birkfellner W, Richter C, Wagenaar D, et al. Dosimetric characteristics of 3D-printed and epoxy-based materials for particle therapy phantoms. Front Phys 2024;12. https://doi.org/10.3389/fphy.2024.1323788.

12. Ozsoykal I, Yurt A. Introduction of a Novel Technique in Density-Adjusted 3D Printing for the Manufacture of Soft-Tissue-Equivalent Radiological Phantoms. Applied Sciences (Switzerland) 2024;14. https://doi.org/10.3390/app14020509.